JOURNAL OF MATERIALS SCIENCE 33 (1998) 2171–2177

Crystallization of $(Fe,Co)_{78}Si_9B_{13}$ alloys: influence of relaxation processes

J. FILIPECKI, Z. MANDECKI
Institute of Physics, Pedagogical University, Al. Armii Krajowej 13/15, 42201 Czestochowa, Poland

C. F. CONDE, A. CONDE
Departamento de Física de la Materia Condensada, Instituto de Ciencia de Materiales, CSIC - Universidad de Sevilla, Apartado 1065, 41080 Sevilla, Spain
E-mail: conde@cica.es

Crystallization of $Fe_{78-x}Co_xSi_9B_{13}$ amorphous alloys has been studied by differential scanning calorimetry (DSC), thermomagnetic gravimetry and X-ray diffraction techniques. Thermal stability of the amorphous alloy monotonically decreases with increasing cobalt content. The devitrification process as detected by DSC occurs in two main stages partially overlapping in temperature, but magnetic characterization reveals a third stage for cobalt-rich alloys. Primary precipitation of α-(Fe, Co) is followed by a polymorphic reaction to give $(Fe,Co)_2B$ phase. Fe_3B-type phase is also detected at the end of the first crystallization stage for iron-rich alloys and β-Co(Si) and Co_2B phases are found in fully crystallized samples for $x = 60$. The influence of relaxation processes on the crystallization was investigated, but no significant effects of pre-annealing on the crystallization parameters resulted.

1. Introduction

Iron- and cobalt-based metallic glasses have been investigated extensively in the last few years because of their magnetic, mechanical and chemical properties. Amorphous to crystalline transformation of these alloys is interesting, not only from the point of view of understanding the crystallization mechanisms, but because it is connected with the changes involved in physical and chemical properties which determine most applications [1, 2]. Annealing of metallic glasses below the crystallization temperature produces various irreversible changes (the so-called structural relaxation) and many of the physical properties change, some drastically and others only to a moderate degree [3, 4].

As previously stated [5, 6], for FeCoSiB amorphous alloys the relaxation processes can be separated into two types: (a) chemical short-range ordering (CSRO), including reversible changes in the local surroundings, which can be described by the activation energy spectrum (AES) model [7, 8], and (b) topological short-range ordering (TSRO), including an irreversible decrease in the free volume, which can be quantitatively described in terms of the free volume model [9, 10].

In this paper we report a characterization of the crystallization processes in $(Fe,Co)_{78}Si_9B_{13}$ glasses by a complementary use of calorimetry (DSC), thermomagnetic (TMG) measurements and X-ray diffraction. To investigate the influence of the relaxation processes in the devitrification transformation of the alloys, as-cast and two types of pre-annealed samples were studied: (a) CSRO samples, pre-annealed for 10^5 s at 530 K, and (b) TSRO samples, annealed for 10^5 s at 578 K, after pre-annealing of 10^5 s at 530 K.

2. Experimental procedure

Metallic glass ribbons 15 mm wide and 15 μm thick with nominal compositions $Fe_{78-x}Co_xSi_9B_{13}$ ($x = 12, 20, 30, 40, 50, 60$) were prepared by a melt-spinning technique at the Institute of Materials Technology of the Warsaw Polytechnic (Poland). Pre-annealing of samples was carried out in a furnace under an argon atmosphere.

Differential scanning calorimetry (DSC) curves, up to 1000 K, were obtained in a Perkin–Elmer DSC-7 under an argon stream. Both temperature and enthalpy calibrations were checked by using lead and K_2CrO_4 standards. In all experiments, samples were heated at the maximum available rate (200 K min^{-1}) from room temperature up to 150 K below the crystallization onset to prevent unwanted annealing. After that, the scan continued at the selected heating rate, in the range 2.5–40 K min^{-1}.

For thermomagnetic (TMG) experiments, the magnetic field of a small magnet was applied to the sample and the temperature variation of the magnetic force was recorded as an apparent weight change of the

sample. Previous calibration of the Perkin–Elmer TGA-7 thermobalance was checked by using the Curie points of nickel, perkalloy and iron standards.

X-ray diffraction spectra were recorded with MoK_α radiation on a DRON 2.0 diffractometer at a scanning step of 0.4° in 2 θ. The working conditions were 40 kV and 20 mA. To allow direct correlation of the phase composition with the calorimetric and thermomagnetic results, XRD scans were made at room temperature on samples previously heated in a furnace under the same experimental conditions.

3. Results and discussion

3.1. Calorimetry

DSC dynamic scans, at a constant heating rate of $10\,K\,min^{-1}$, for as-quenched samples of $Fe_{78-x}Co_xSi_9B_{13}$ alloys are shown in Fig. 1. As can be observed, amorphous to crystalline transformation for the studied alloys consists of at least two steps as revealed by the two temperature-resolved exotherms in the DSC scans. Measured values of peak temperature, T_p, and enthalpy, ΔH, of the two exotherms are listed in Table I. For the lower cobalt content alloys, showing partial temperature overlapping of the two DSC maxima, the value of the enthalpy attributed to either step was calculated from an approximate deconvolution of the two exotherms.

Thermal stability of the amorphous alloy against crystallization, monotonically decreases with the cobalt content in the glass, as evidenced by the shift of the crystallization onset to lower temperatures. On the other hand, the temperature interval between the two crystallization stages increases with the cobalt content, and so the partial overlapping of the two exotherms in the DSC scans for the lowest cobalt content alloys, gradually disappears as the cobalt percentage in the alloy increases. Fig. 2 illustrates the composition dependence of the crystallization temperatures. As observed, T_{p1} decreases almost linearly upon increasing the cobalt concentration, the value found for the slope from a linear fit being about 0.6 K/at% Co. This behaviour agrees with the reported results for analogous iron, cobalt based alloys with compositions $(FeCo)_{78}Si_{10}B_{12}$ [11] and $(FeCo)_{77}Si_{10}B_{13}$ [12], but in contrast to the observed behaviour of $(FeCo)_{78}Si_8B_{14}$ [13] and $(FeCo)_{62.5}Si_{12.5}B_{25}$ [14] alloys in which the substitution of cobalt for iron results in an enhancement of thermal stability. For the second crystallization stage, the peak temperature value is essentially the same, i.e. 830 K, showing no significant composition dependence.

Fig. 3 illustrates the composition dependence of the enthalpy of the two crystallization steps. As shown, the more significant composition dependence is found for the second-step enthalpy, showing variations up to above 40% from the mean value. The smallest enthalpy values correspond to the low cobalt content alloys, to rise abruptly up to a maximum for the $x = 30$ at % Co alloy and gradually to decrease for higher cobalt content alloys. For the first crystallization step, the enthalpy shows smaller variations

TABLE I Crystallization parameters for as-quenched $Fe_{78-x}Co_xSi_9B_{13}$ alloys

	x					
	12	20	30	40	50	60
T_{onset} (K)	804	797	792	781	780	775
T_{p1} (K)	811	806	800	790	789	782
T_{p2} (K)	828	833	834	834	831	833
ΔH_1 ($kJ\,mol^{-1}$)	92	85	77	90	81	60
ΔH_2 ($kJ\,mol^{-1}$)	36	53	88	71	65	62
E_1 (eV)	3.7	4.0	3.8	3.5	3.8	4.3
E_2 (eV)	3.1	3.7	3.7	3.6	3.6	4.2

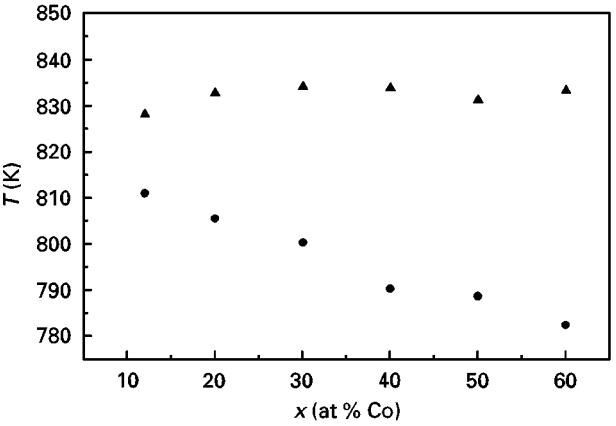

Figure 2 Composition dependence of the crystallization temperatures, (●) T_{p1} and (▲) T_{p2}, for $Fe_{78-x}Co_xSi_9B_{13}$ as-cast alloys.

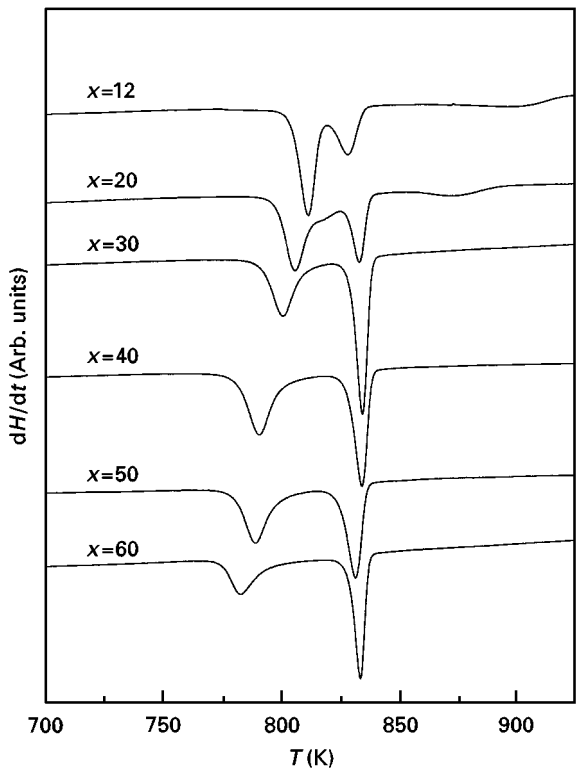

Figure 1 DSC curves during continuous heating at $10\,K\,min^{-1}$ of $Fe_{78-x}Co_xSi_9B_{13}$ as-cast glasses.

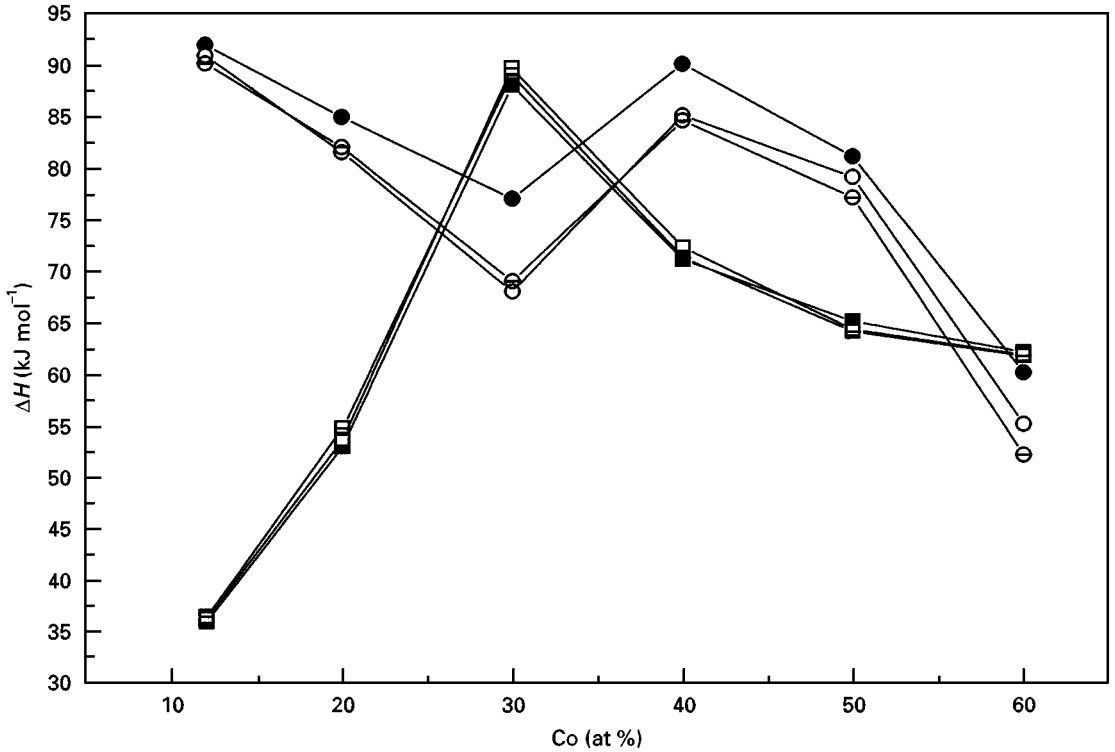

Figure 3 Crystallization enthalpy values of the two crystallization stages for (●, ■) as-quenched and (○, ⊖, □, ⊟) pre-annealed $Fe_{78-x}Co_xSi_9B_{13}$ samples. $\triangle H_1$: (○) CSRO, (⊖) TSRO. $\triangle H_2$: (□) CSRO, (⊟) TSRO.

(<15% from the mean value) and decreases with increasing cobalt content, except for a significant increase for alloys of intermediate compositions ($x = 30$–40).

DSC scans for partially crystallized samples (previously heated up to the first exotherm peak temperature and abruptly cooled to room temperature) exhibit a single exotherm, in the same temperature range as the second exotherm in the DSC scans for as-quenched samples, and no significant variations in enthalpy values are found. This result should indicate the independent character of the two crystallization stages.

For samples pre-annealed for 10^6 s at 530 K (CSRO samples) and for those isothermally treated for 10^6 s at 530 K and, after that, for 10^6 s at 578 K (TSRO samples), DSC dynamic scans are completely similar to those obtained for as-quenched samples for all compositions and crystallization temperature values are only slightly higher ($\Delta T_p \lesssim 2$ K). Values of the crystallization enthalpy for CSRO and TSRO samples do not show important variations from those found for as-quenched samples, although a small decrease ($\lesssim 5\%$) in the enthalpy of the first crystallization stage in CSRO and TSRO samples is found, as illustrated in Fig. 3. As can be expected, no variations in the enthalpy of the second stage occur for CSRO and TSRO samples.

The activation energy of each crystallization stage was evaluated from the shift of the crystallization peak temperature, T_p, with the heating rate, β (in the range 2.5–40 K min^{-1}), by using Kissinger's relation [15]

$$d[\ln(\beta/T_p^2)]\, d(1/T_p) = -E/R \qquad (1)$$

where R is the gas constant.

Kissinger plots for the two crystallization stages are linear, indicating that kinetics of the crystallization processes in these alloys are of the first order. Values found for the activation energy are listed in Table I. For the first step, the activation energy shows a minimum for the 40 at % Co alloy and a significant increase occurs for the cobalt-rich alloys. Activation energy of the second crystallization step also shows the highest value for the 60 at % Co alloy, but it is nearly constant for the composition range 20–50 at % Co, and significantly decreases for the 12 at % Co alloy.

No significant variations in activation energy values are found for CSRO and TSRO samples with respect to the as-quenched samples of the same alloy composition. This result agrees with that mentioned above that there is a small effect of pre-annealing on the values of crystallization temperatures and enthalpies.

The Avrami index value allows a primary approach to the involved mechanisms in the crystallization reactions. An estimation of the Avrami index, n, can be made by using the maximum reaction rate equation derived by Gao and Wang [16]

$$(dx/dt)_p = 0.37nK_p \qquad (2)$$

where $(dx/dt)_p$ is the maximum crystallization rate at the peak and $x(t)$ is the transformed volume fraction at time t, and $K_p = \beta E/RT_p^2$ is called the rate constant.

From the linearity exhibited by plots of $(dx/dt)_p$ versus β/T_p^2, we can conclude that n is independent of the heating rate, at least in the explored range $2.5 \leqslant \beta \leqslant 40$ K min^{-1}. Values of the Avrami exponent derived from the above plots are near 2.5 for the first crystallization stage and range between 4 and 5 for the second stage.

An unambiguous interpretation of the crystallization kinetics is difficult when microscopic observations are not available because of the possibility of several kinds of sites with different nucleation rates and modes of growth. Additional difficulty arises from the presence of two or more crystalline phases, as evidenced in the present study from the X-ray results. However, it may be helpful to examine the kinetic results in the light of an approximate model [17]. Here, it is assumed that $n = a + bp$, where a accounts for the nucleation rate and varies from zero (for quenched-in nuclei) to 1 (for a constant nucleation rate), b defines the dimensionality of the growth ($b = 1, 2$ or 3), p has value of 1 for interfacial control of growth (assumed linear in time), and $p = 0.5$ for diffusion-controlled growth.

Thus, value $n_1 = 2.5$ points to three-dimensional diffusion-controlled growth with constant nucleation rate, as expected for a primary crystallization. This value of the Avrami exponent is usually found for the first crystallization stage of MSiB (M = Fe, Co) metallic glasses. For the second crystallization stage, $n = 4$ should suggest three-dimensional interface-controlled growth with a constant nucleation rate, as found for analogous metallic glasses.

3.2. Thermomagnetic measurements

Plots of low-field magnetization (in arbitrary units) as a function of temperature for as-quenched samples of the studied alloys, at a heating rate of 40 K min^{-1}, are shown in Fig. 4a–f, (curves 1). TMG plots for pre-annealed CSRO and TSRO samples are similar to those obtained for as-quenched samples and no significant variations should be noted.

Apart from some differential details, considered below, TMG curves are qualitatively similar for all the alloys and the following general features should be noted. The first fall in magnetization corresponds to the transition from an amorphous ferromagnetic to an amorphous paramagnetic state. This temperature is identified as the Curie temperature of the as-cast glassy phase. At a higher temperature, corresponding to the crystallization onset, samples exhibit an increase in magnetic moment, indicating the formation of crystalline phases that are ferromagnetic, with Curie temperatures higher than that of crystallization. Finally, the transition ferro–paramagnetic of crystalline phases is evinced by the fall to zero of the magnetization.

The values of the Curie temperature of the initial amorphous material as a function of the cobalt concentration are shown in Fig. 5. As observed, T_c significantly increases from the 12 at % Co alloy to the 20 at % Co alloy, to maintain a nearly constant value, with only a slight decrease as the cobalt content increases for more cobalt-rich alloys. This behaviour of the Curie temperature of the amorphous alloy versus cobalt content agrees well with the reported results for alloys of similar compositions: $(FeCo)_{78}Si_{10}B_{12}$ [11] and $(FeCo)_{78}Si_9B_{13}$ [18].

As obtained from the DSC experiments, the crystallization onset temperature is shifted to lower temperatures by increasing the cobalt content of the alloy, occurring at a temperature lower than the Curie transition of the amorphous phase making it impossible to observe the beginning of the rise in magnetic moment associated with the crystallization. This fact results in a non-zero residual magnetization at that Curie transition, as a result of the superposition of two opposite effects: the fall to zero in magnetization of the amorphous matrix, and the increase in the magnetic moment due to the volume fraction of the crystalline ferromagnetic phases already formed at that temperature. Effectively, it is observed that the value of residual magnetization at the Curie point increases with the cobalt content of the alloy (up to $x = 40$ at %), as a consequence of a more advanced state of the first crystallization stage. However, for more cobalt-rich alloys, that residual M value decreases, indicating a smaller volume fraction of the crystalline magnetic phase formed in the first devitrification stage; this result agrees with a smaller value of the enthalpy associated to the first exotherm in these alloys (Table I).

Crystallization behaviour, as revealed by TMG curves, is complicated and tends to be different from sample to sample, depending on the chemical composition. As can be observed in curves 1 of Fig. 4a–f, two or three crystallization steps are revealed by broad and sharp changes in magnetization. However, some deductions could be extracted by correlating the thermal evolution of the magnetic moment of the different alloys and the corresponding DSC curves and X-ray results.

For iron-rich alloy ($x = 12$), $M(T)$ plots exhibit similar features to those usually found for FeSiB alloys: a two-stage rise in magnetic moment, associated with the two DSC exotherms, that should correspond to a primary precipitation of α-Fe(Co, Si) phase and a polymorphic reaction to give $(Fe, Co)_2B$ phase, respectively. The metastable Fe_3B-type phase formed during the first stage makes no contribution to magnetic moment, because crystallization occurs in the paramagnetic region of that phase. For $x = 20, 30, 40$, and 50, a three-stage crystallization is in evidence in $M(T)$ plots: the first and second stages are analogous to those described above for iron-rich alloys, but the plot appearance is changed because the crystallization starts below the Curie temperature of the amorphous alloy. On the other hand, the second stage starts near the paramagnetic region of the $(Fe, Co)_2B$ phase, the Curie temperature of which gradually decreases with the cobalt content. However, the more significant change in $M(T)$ plots of these alloys is the presence of a third stage, evinced as a rise in the magnetic moment starting at a temperature (in the range 875–1000 K), that decreases with the cobalt content of the alloy. This feature has no corresponding form in the DSC curves, which do not show visible deviation from the base line in that temperature range, and X-ray records for samples heated below and above that temperature do not show qualitative changes. So, the rise in the magnetic moment should be attributed to some recrystallization process involving the magnetic phases so far formed. Finally, for $x = 60$,

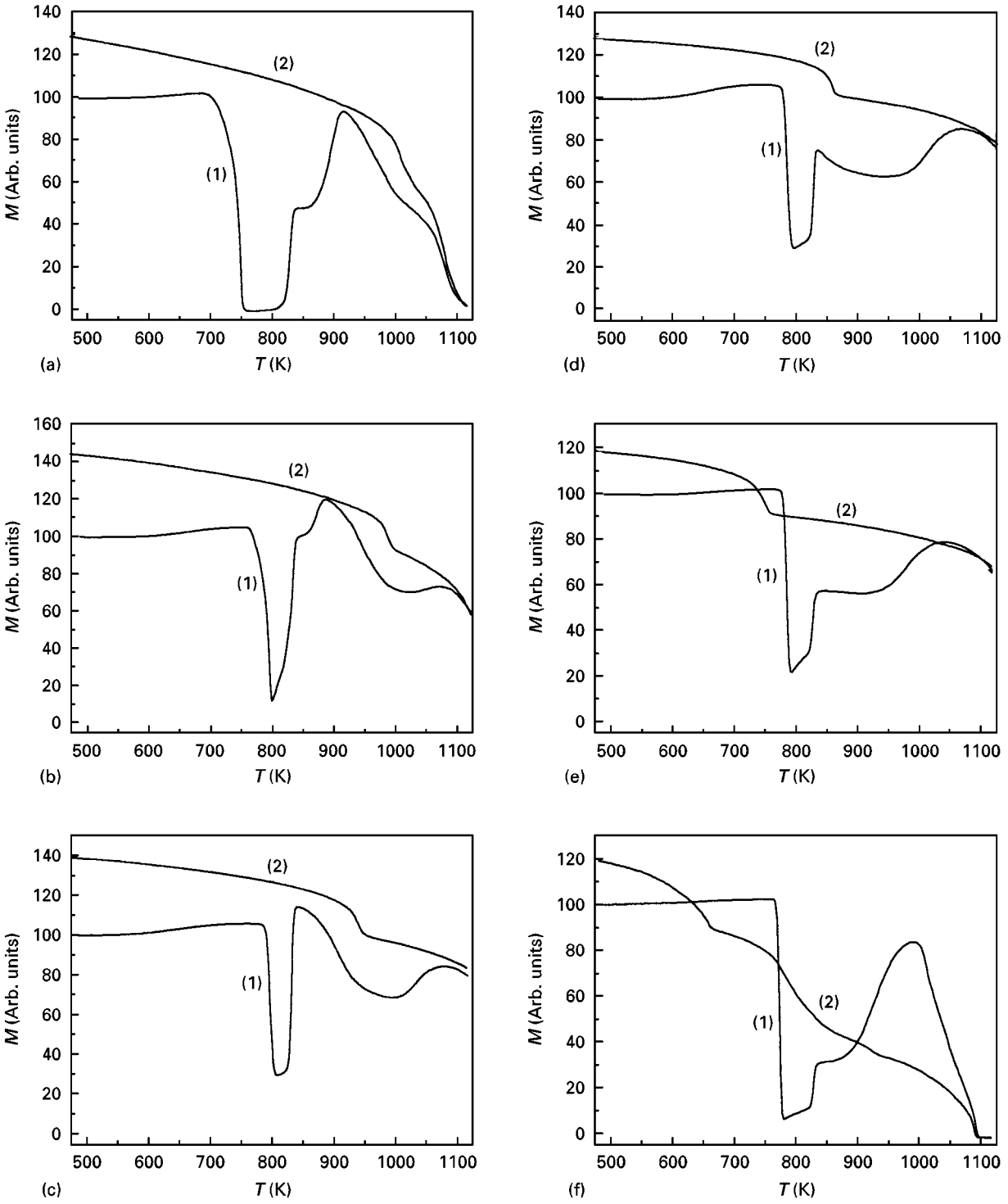

Figure 4(a–f) Thermomagnetic plots, at 40 K min^{-1}, for as-quenched (curves 1) and crystallized (curves 2) of $Fe_{78-x}Co_xSi_9B_{13}$ alloys. x: (a) 12, (b) 20, (c) 30, (d) 40, (e) 50, (f) 60.

a three-stage process is also present, but the existence of two steps in the fall to zero of magnetization at higher temperature evinces two magnetic phases with Curie temperatures around 1050 and 1100 K, respectively, that should correspond to the α-Fe(Co, Si) and Co(Si) phases shown in the X-ray record of fully crystallized samples for this alloy composition.

For fully crystallized samples, TMG plots (curves 2 in Fig. 4a–f) show a two-stage fall to zero of magnetic moment that indicates the ferro-paramagnetic transition of the two final phases: $(Fe, Co)_2B$ and α-Fe(Co, Si). As can be observed in Fig. 5, the Curie temperature of the Fe_2B-type phase drops almost linearly with increasing cobalt content, the slope being about -10 K at % Co. For $x = 60$, a three-stage fall to zero in magnetization is found, the intermediate step corresponding to the Curie transition of the Co_2B phase.

3.3. X-ray diffraction

Amorphous to crystalline transformation of the alloys was structurally characterized by X-ray diffraction. Fig. 6 shows the significant portions of diffractometric

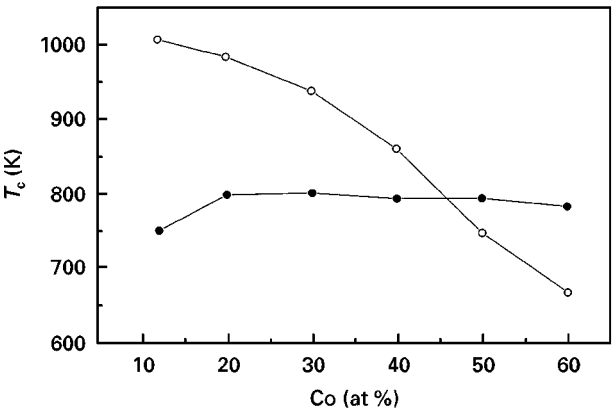

Figure 5 Curie temperature of (●) the amorphous as-cast and (○) $(Fe,Co)_2B$ final crystalline phase, as a function of cobalt content.

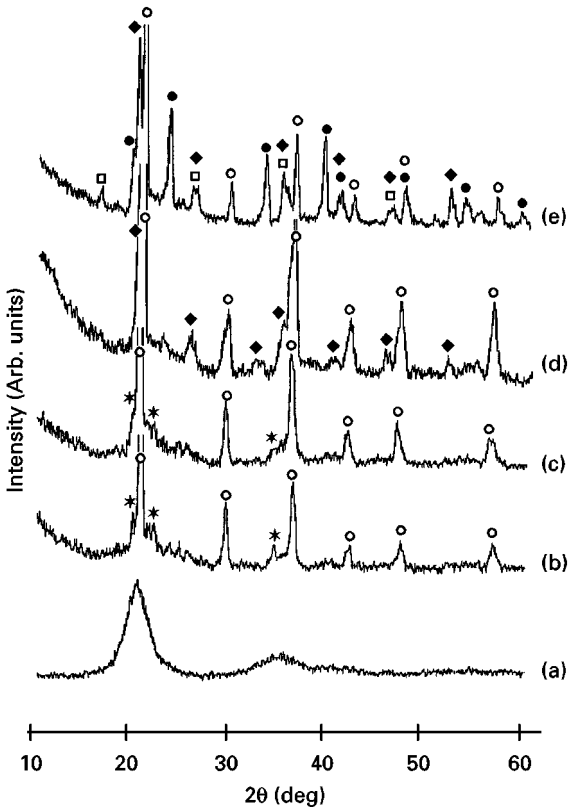

Figure 6 X-ray diffraction patterns at different stages of the transformation: (a) amorphous ($x = 50$); (b) $x = 12$ alloy heated up to 810 K (first crystallization stage); (c) $x = 20$ alloy at the same conditions as (b); (d) $x = 50$ alloy heated up to 1100 K (second stage); (e) $x = 60$ alloy at the same conditions as (d). (○) α-Fe, (●) β-Co, (◆) $(Fe,Co)_2B$, (□) Co_2B, (★) Fe_3B.

records of as-cast and several heat-treated samples. For as-quenched samples, the amorphous state is manifested by the typical broad intensity maximum at diffraction angles $2\theta(MoK_\alpha)$ around 20° (Fig. 6a). Samples partially crystallized (previously heated up to the first DSC exotherm) show (Fig. 6b) the presence of some crystalline lines identified as belonging to a b c c solid solution α-Fe(Co, Si). In addition to the crystalline lines, the X-ray pattern for these samples shows the broad peak due to the remaining amorphous phase. For iron-rich alloys ($x = 12$–30), other lines assigned to an orthorhombic Fe_3B-type phase were also observed (Fig. 6c), indicating the gradual appearance of this metastable phase by increasing the iron content of the alloy. The presence of a Fe_3B-type phase in partially crystallized FeCoSiB alloys with low cobalt content has been previously reported from X-ray and electron microscopy studies [18–22].

The second stage corresponds to a polymorphic reaction that fully crystallizes the amorphous matrix. The transformation of the metastable Fe_3B-type phase to the equilibrium α-Fe and Fe_2B type phases also occurs. The two major final products of the crystallization are α-Fe(Co, Si) and body-centred tetragonal $(Fe,Co)_2B$ phases (Fig. 6d), as is usually found for FeCoSiB alloys [18, 20, 22–24]. For the alloy containing the highest cobalt concentration ($x = 60$) the presence of the Co_2B phase was detected after crystallization (Fig. 6e), as is evident from TMG results. However, that phase was not detected for alloys with a smaller cobalt content as reported by Mathur *et al.* [20]. Finally, the presence of β-Co(Si) phase in fully crystallized samples of the $x = 60$ alloy should be noted. The presence of β-Co phase in the crystallization of the low-iron content FeCoB alloys has been reported previously [25].

4. Conclusion

The thermal stability of the $(Fe,Co)_{78}Si_9B_{13}$ alloys studied monotonically decreases with the cobalt content and an almost linear drop of the crystallization onset temperature was found. The Curie temperature of the amorphous alloy increases with cobalt content up to $x = 20$ to maintain a nearly constant value for $20 < x < 60$.

The continuous heating crystallization is shown as two resolved DSC exotherms, partially overlapping in temperature for iron-rich alloys, but is detected by magnetic measurements and seen to proceed in two and, in some cases, three steps. Primary precipitation of α-Fe(Co, Si) phase is followed by the formation of the Fe_3B phase. Then, a polymorphic reaction occurs and the two major final products are α-Fe(Co, Si) and $(Fe,Co)_2B$ phases.

Pre-annealing of the sampling does not significantly affect the crystallization parameters: only the crystallization onset is slightly delayed with respect that of as-quenched samples, but no appreciable changes in enthalpy or activation energy were found. Thus, relaxation processes do not significantly influence the crystallization processes in these alloys.

Acknowledgements

This work was supported by the CICYT of the Spanish Government (Project MAT95-0961-CO2-01) and the PAI of the Junta de Andalucía. J. Filipecki thanks the University of Seville for allowing the research stay, and the Committee of the UE Commission in Brussels for a Tempus Fellowship.

References

1. F. E. LUBORSKY (Ed.), "Amorphous Metallic Alloys" (Butterworths, London, 1983).

2. T. R. ANATHARAMAN (Ed.), "Metallic Glasses: Production, Properties and Applications" (Trans. Tech. Aedermannsderg, Switzerland, 1984).
3. A. van den BEUKEL, in "Rapidly Solidified Materials", edited by P. W. Lee and S. Carbonera (ASM, New York, 1986) p. 193.
4. A. L. GREER, in "Rapidly Solidified Alloys: Processes, Structure, Properties, Applications", edited by H. H. Liebermand (New York, 1993) p. 269.
5. J. FILIPECKI and A. van den BEUKEL, *Scripta Metall.* **22** (1987) 1111.
6. *Idem*, *J. Mater. Sci. Lett.* **9** (1990) 1160.
7. M. R. J. GIBBS and J. E. EVETTS, in "Proceedings of the 4th International Conference on Rapidly Quenched Metals", edited by T. Matsumoto and K. Suzuki (Sendai, 1982) pp. 479, 513.
8. M. R. J. GIBBS, J. E. EVETTS and J. A. LEAKE, *J. Mater. Sci.* **18** (1983) 419.
9. F. SPAEPEN, Acta Metall. **25** (1977) 419.
10. A. van den BEUKEL and S. RADELAAR, *ibid.* **31** (1983) 419.
11. H. FUJIMORI, H. MORITA, Y. OBI and S. OTHA, in "Amorphous Magnetism II", Proceedings of the 2nd International Symposium on Amorphous Magnetism, edited by R. A. Levy and R. Hasegawa (Plenum, New York, 1977) p. 393.
12. G. MITITA, T. HATSUO and T. HOSHIKIKO, *Jpn J. Appl. Phys.* **17** (1978) 1877.
13. Y. C. KUO, L. S. ZHANG and W. K. ZANG, *J. Appl. Phys.* **52** (1981) 1889.
14. B.-G. SHEN, L. CAO and H.-Q. GUO, *ibid.* **73** (1993) 5730.
15. H. E. KISSINGER, *J. Res. NBS* **57** (1956) 217.
16. Y. Q. GAO and W. WANG, *J. Non-Cryst. Solids* **81** (1986) 129.
17. V. R. V. RAMANAN and G. FISH, *J. Appl. Phys.* **53** (1982) 2273.
18. G. A. STERGIOUDIS, J. YANKINTHOS, P. J. RENTZEPERIS, Z. BOJARSKI and T. J. PANEK, *J. Mater. Sci.* **27** (1992) 2468.
19. E. G. BABURAJ, G. K. DEY, M. J. PATNI and R. KRISHNAN, *Scripta Metall.* **19** (1985) 305.
20. R. P. MATHUR, V. N. MURTHY, D. AKHTAR, P. SUBRAHMANIAN and R. JAGANNATHAN, *J. Mater. Sci.* **6** (1987) 1019.
21. M. MILLÁN, J. LEAL and A. CONDE, *Mater. Lett.* **14** (1992) 227.
22. C. F. CONDE, M. MILLÁN and A. CONDE, *Key Eng. Mater.* **81-83** (1993) 311.
23. T. NAGARAJAN, U. CHIDAMBARAN ASSARI, S. SRINIVASAN, V. SRIDHARAN and A. NARAYANASAMY, *Mat. Sci. Eng.* **97** (1988) 355.
24. M. L. TRUDEAU, J-Y. HUOT and R. SCHULZ, *J. Appl. Phys.* **67** (1990) 2333.
25. P. DUHAJ, P. SVEC, M. DURCEKOVA and G. VLASAK, *Mater. Sci. Eng.* **97** (1988) 337.

Received 10 October 1996
and accepted 17 December 1997